JOC The Journal of Organic Chemistry

Note

pubs.acs.org/joc

Bingel–Hirsch Addition on Non-Isolated-Pentagon-Rule $Gd_3N@C_{2n}$ ($2n$ = 82 and 84) Metallofullerenes: Products under Kinetic Control

Núria Alegret, Patricia Salvadó, Antonio Rodríguez-Fortea,* and Josep M. Poblet*

Departament de Química Física i Inorgànica, Universitat Rovira i Virgili, c/Marcel·lí Domingo s/n, 43007 Tarragona, Spain

Supporting Information

ABSTRACT: Bingel–Hirsch reactions on fullerenes take place under kinetic control. We here predict, by means of DFT methodology, the products of the Bingel–Hirsch addition on non-isolated-pentagon-rule (non-IPR) metallofullerenes $Gd_3N@C_{2n}$ ($2n$ = 82, 84), as modeled by closed-shell $Y_3N@C_{2n}$ systems. Adducts on [6,6] B-type bonds placed near the pentalene unit are predicted for the two cages, as found for other non-IPR endohedral fullerenes such as $Sc_3N@C_{68}$.

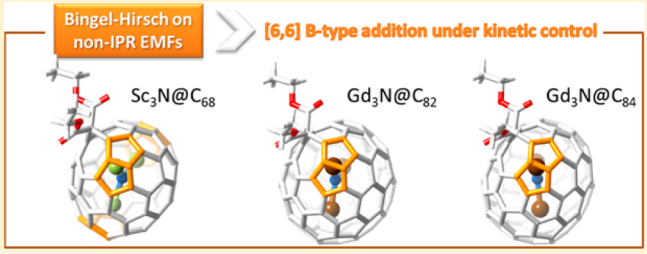

Endohedral metallofullerenes (EMFs) have attracted broad interest in the past decade because of their unique properties that make them molecules with potential applications in many fields such as molecular electronics or nanomedicine.[1−4] Exohedral functionalization is in general required to take full advantage of these compounds. Cycloaddition reactions have been important in the development of EMF derivatives.[5] The small amounts of EMF reactants along with the low yields for these reactions lead to almost invisible amounts of products at the submilligram level, which are very difficult to characterize in the laboratory. Computational chemistry here plays an important role as a complementary technique for such a characterization process.[6] Predictions about the regioselectivity of a reaction on a given EMF made from structural or topological parameters of the carbon cage are possible, but an exhaustive analysis of the potential energy surface is required in most cases.[7−9]

The Bingel–Hirsch reaction is a type of nucleophilic [2 + 1] cycloaddition in which a bromomalonate reacts with a fullerene cage.[10] According to Scheme 1, the Bingel–Hirsch reaction takes place in two separate steps. In the first one, a charged intermediate with the bromomalonate attached to a C atom of the fullerene is formed through an almost barrierless process. After that, a bromide anion is released and a second bond between the malonate and the cage is formed. Echegoyen and coworkers have used the Bingel–Hirsch reaction to derivatize the non-isolated-pentagon-rule (non-IPR) EMFs $Gd_3N@C_s(39663)$-C_{82} and $Gd_3N@C_s(51365)$-C_{84}, among others.[11,12] For the C_{82} cage, three different monoadducts with relative amounts of 90%, 7%, and 3% were isolated. For the C_{84} cage, a single monoadduct was isolated experimentally by HPLC, and several multiadducts were detected. An extensive computational study based on the relative stabilities of the reaction products was also done to rationalize the regioselectivity observed with these two non-IPR EMFs.[13] Recent results by our group, however, showed that the Bingel–Hirsch addition on EMFs takes place under kinetic rather than thermodynamic control,[8] as for the first available fullerene oxides $C_{60}O$ and $C_{60}O_2$.[14] On that basis, in the present work we used density functional theory (DFT) (see Computational Methodology) to perform a thorough exploration of the reaction profiles for the Bingel–Hirsch additions on $Gd_3N@C_s(39663)$-C_{82} and $Gd_3N@C_s(51365)$-C_{84} that complements our previous studies. Products that should be observed under kinetic control are proposed.

Scheme 1. General Mechanism of the Bingel–Hirsch Reaction

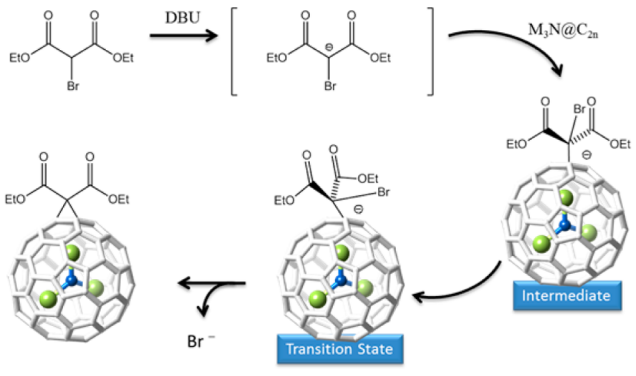

As already noted, the structures of $Gd_3N@C_s(39663)$-C_{82} and $Gd_3N@C_s(51365)$-C_{84} are rather similar (see Figures S1 and S2 in the Supporting Information).[15,16] Both are non-IPR cages that contain one adjacent pentagon pair (i.e., a pentalene motif) with one of the internal Gd ions pointing to it. The two carbon cages, with C_s symmetry, have 67 (C_{84}) and 66 (C_{82}) different C–C bonds. We assumed pseudo-C_s symmetry for the two EMFs studied here because the plane of the Gd_3N cluster is near the σ_h plane of the cages. Rotation of the internal cluster is another important issue that has to be considered in this type of analysis.

Received: July 12, 2013
Published: September 4, 2013

   dx.doi.org/10.1021/jo4014832 | J. Org. Chem. 2013, 78, 9986–9990

Only those orientations with one Gd^{3+} ion directed toward the pentalene unit were selected for each regioisomer and intermediate because of the limited rotation of the Gd_3N cluster in these cages.[13] As performed and validated previously,[13,17] we considered a model in which Gd^{3+} was replaced with Y^{3+} because calculations with metals that have unfilled 4f shells are not yet routine. The products under kinetic control for the Bingel–Hirsch reaction on $Sc_3N@C_{2n}$ ($2n$ = 80, 68) are adducts on [6,6] B-type bonds near the pentalene unit (Figure S4 in the Supporting Information).[8] For the IPR C_{80} cage, the intermediate was formed on a 666 atom (i.e., an atom surrounded by three hexagons), while for the non-IPR C_{68} cage it was formed in one of the 566 atoms of the pentalene unit. On the basis of those results, in this study we analyzed (i) all of the different bonds around the pentalene region and (ii) all of the B-type bonds near the metal atoms, taking into account the restricted rotation of the internal cluster. For the intermediates with the lowest energies, which are highlighted in bold in Figure 1, we computed the associated transition states (TSs). It should be noted that bonds are named with letters while atoms are labeled with numbers. Thus, for example, we can identify the intermediate/TS **74g** of the $Y_3N@C_{82}$ cage as the one in which the malonate is bonded to atom 74 and oriented to form product **g** (i.e., the adduct over bond **g**).

The results are collected in Table 1 (a complete list of all the results is presented in Table S1 in the Supporting Information). For $Y_3N@C_s(39663)$-C_{82}, the four products **b**, **f**, **a**, and **e** are almost isoenergetic within the error of the methodology, with relative energies of 0.0, 0.3, 0.5, and 0.7 kcal mol^{-1}, respectively. It should be noted that all four of these adducts are on corannulene-type bonds located around the pentalene motif (Figure 1). Moreover, the four bonds show very similar structural parameters according to their symmetry equivalence. Because of the reduced rotation of the nitride around the N–Y–pentalene axis, we considered only the adducts on bonds **j** and **k** among the bonds that are far from the pentalene unit (Figure 1). Products **j** and **k** are 5.2 and 6.4 kcal mol^{-1} higher in energy than **b**, respectively. Product **g** is close in energy to them, at 6.1 kcal mol^{-1}. The energy difference between this first set of monoadducts and the rest of the possible regioisomers is more than 11 kcal mol^{-1} (see Table 1 and Table S1 in the Supporting Information). Results are analogous to those already found using different computational settings.[13]

We analyzed the different intermediates that lead to these products (Table 1). The most stable intermediate **81b** is the one that leads to the most stable product. Intermediates **81c** and **81h**, which are directly related to **81b** by 120° rotation around the formed C_{fuller}–$C_{malonate}$ axis, are 0.7 and 2.4 kcal mol^{-1} higher (see Figure S5 in the Supporting Information). Intermediates **74g** and **40k** are found at 1.1 and 1.2 kcal mol^{-1} with respect to **81b**. Finally, we found a set of different type of intermediates in the range between 1.9 and 2.5 kcal mol^{-1}. It should be noted that the energy differences among the intermediates are not as significant as those found among the products. The TSs for the lowest-energy intermediates were also computed (Table 1). From intermediate **74g**, the formation of the product on bond **g** requires overcoming an activation barrier of 13.7 kcal mol^{-1} (the energy of the TS is −2.1 kcal mol^{-1} relative to reactants; Table 1 and Figure 2). The second-lowest-energy TS, **81h**, was 4.5 kcal mol^{-1} higher. TSs **49j**, **81c**, and **68i** are located within 6 kcal mol^{-1} of **74g**. The rest of the computed TSs lie more than 6 kcal mol^{-1} higher than **74g**. In general, the lowest-energy TSs are those that lead to [6,6] B-type products. Furthermore, near the pentalene unit, the TSs formed on 566 atoms are favored, while far from the pentalene, those formed on 666 atoms are preferred. We can explain these results because addition onto a 566 atom near the [5,5] region releases more surface strain than addition onto a 666 atom, as found for other EMFs.[8,18] Thus, we propose that if the Bingel–Hirsch reaction were to happen under kinetic control on $Y_3N@C_s(39663)$-C_{82}, the most abundant monoadduct should be product **g**, which shows the lowest-energy TS (Figure 2). We propose that the second most abundant monoadduct, with a yield of 7%, should be product **h**. Finally, three candidates for the third abundant monoadduct are proposed: products **j**, **c**, and **i**.

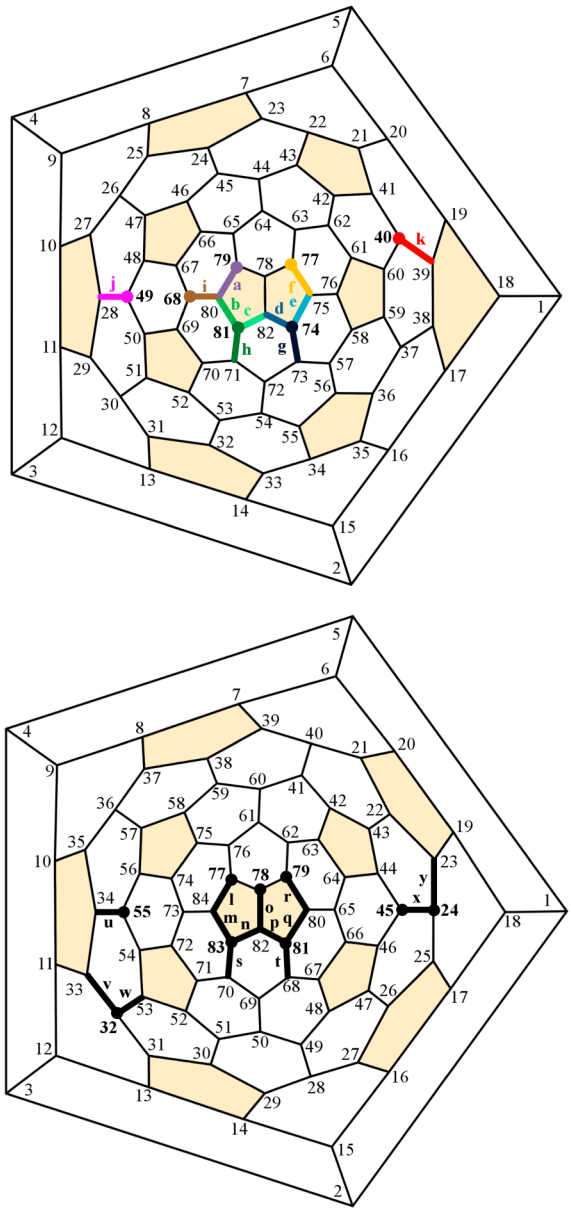

Figure 1. Schlegel diagrams for (top) $C_s(39663)$-C_{82} and (bottom) $C_s(51365)$-C_{84}. The 12 pentagons are colored in orange. The bonds for which the potential energy surface has been studied in detail (intermediates, TSs, and products) are highlighted in bold. The color code for the bonds in the Schlegel diagram for $C_s(39663)$-C_{82} is also used in Figure 2.

The same analysis was performed on $Y_3N@C_s(51365)$-C_{84}. Here the number of possible [6,6] B-type bonds far from the

dx.doi.org/10.1021/jo4014832 | J. Org. Chem. 2013, 78, 9986–9990

Table 1. Energies with respect to reactants for the different computed intermediates, transition states and products of the Bingel–Hirsch addition on $Y_3N@C_{2n}$ ($2n$=82 and 84) including solvent effects (ortho-dichlorobenzene)

product	bond type[a]	intermediate[b]	atom type[c]	E_{rel} intermediate[d]		E_a TS[e]		E_{rel} products[d]	
				$Y_3N@C_s(39663)$-C_{82}					
g	[6,6] type B	**74g**	566	−15.7	(1.1)	−2.1	(13.7)	−32.3	(6.1)
h	[6,6] type B	**81h**	566	−14.5	(2.4)	2.4	(19.2)	−20.6	(17.8)
j	[6,6] type B	**49j**	666	−14.6	(2.2)	3.6	(18.2)	−33.2	(5.2)
c	[5,6] type F	**81c**	566	−16.1	(0.7)	3.9	(20.7)	−20.2	(18.2)
i	[6,6] type B	**68i**	666	−14.4	(2.4)	4.1	(18.5)	−12.6	(25.8)
e	[5,6] corannulene	**74e**	566	−12.8	(4.0)	6.3	(22.0)	−37.7	(0.7)
a	[5,6] corannulene	**79a**	566	−14.3	(2.5)	6.8	(21.0)	−37.9	(0.5)
d	[5,6] type F	**74d**	566	−14.9	(1.9)	6.9	(22.6)	−19.9	(18.5)
b	[5,6] corannulene	**81b**	566	−16.8	(0.0)	8.0	(24.8)	−38.4	(0.0)
k	[6,6] type B	**40k**	666	−15.7	(1.2)	8.7	(24.4)	−32.0	(6.4)
f	[5,6] corannulene	**77f**	566	−14.8	(2.0)	8.8	(23.6)	−38.1	(0.3)
				$Y_3N@C_s(51365)$-C_{84}					
s	[6,6] type B	**83s**	566	−16.6	(0.2)	0.7	(17.3)	−29.6	(12.7)
t	[6,6] type B	**81t**	566	−15.8	(0.9)	2.9	(18.7)	−25.9	(16.4)
n	[5,6] type F	**83n**	566	−14.4	(2.4)	3.4	(20.1)	−23.3	(19.0)
y	[6,6] type B	**24y**	666	−15.0	(1.7)	4.6	(19.6)	−37.6	(4.7)
m	[5,6] corannulene	**83m**	566	−15.1	(1.7)	4.9	(21.5)	−41.6	(0.7)
q	[5,6] corannulene	**81q**	566	−15.4	(1.4)	5.1	(20.5)	−37.3	(5.0)
u	[6,6] type B	**55u**	566	−15.2	(1.6)	5.1	(20.3)	−25.0	(17.3)
l	[5,6] corannulene	**77l**	566	−14.6	(2.1)	5.5	(20.2)	−42.3	(0.0)
r	[5,6] corannulene	**79r**	566	−16.8	(0.0)	5.8	(22.6)	−40.0	(2.3)
p	[5,6] type F	**81p**	566	−14.3	(2.5)	5.9	(21.3)	−20.4	(21.9)
w	[6,6] type B	**32w**	566	−14.6	(2.2)	6.3	(20.7)	−20.0	(22.3)
v	[6,6] type B	**32v**	666	−14.4	(2.4)	6.5	(20.8)	−36.5	(5.8)
x	[6,6] pyrene	**24x**	666	−14.5	(2.3)	7.5	(22.5)	−36.4	(5.9)
o	[5,5] pentalene	**78o**	556	−10.7	(6.0)	9.2	(19.9)	−30.4	(11.9)
x	[6,6] pyrene	**45x**	666	−12.5	(4.3)	10.0	(22.5)	−36.4	(5.9)

[a]Type of bond according to Figure S4 in the Supporting Information. [b]Labels for intermediates: **74g** stands for the intermediate on atom 74 that leads to the adduct on bond **g** (see Figure 1). The labels for the intermediates are also applicable to the TSs. [c]Type of atom forming the intermediate. [d]Relative energies (in kcal mol^{-1}) with respect to reactants and (in parentheses) the most stable intermediate/product. [e]Relative energies of the TS (in kcal mol^{-1}) with respect to reactants and (in parentheses) the corresponding intermediate.

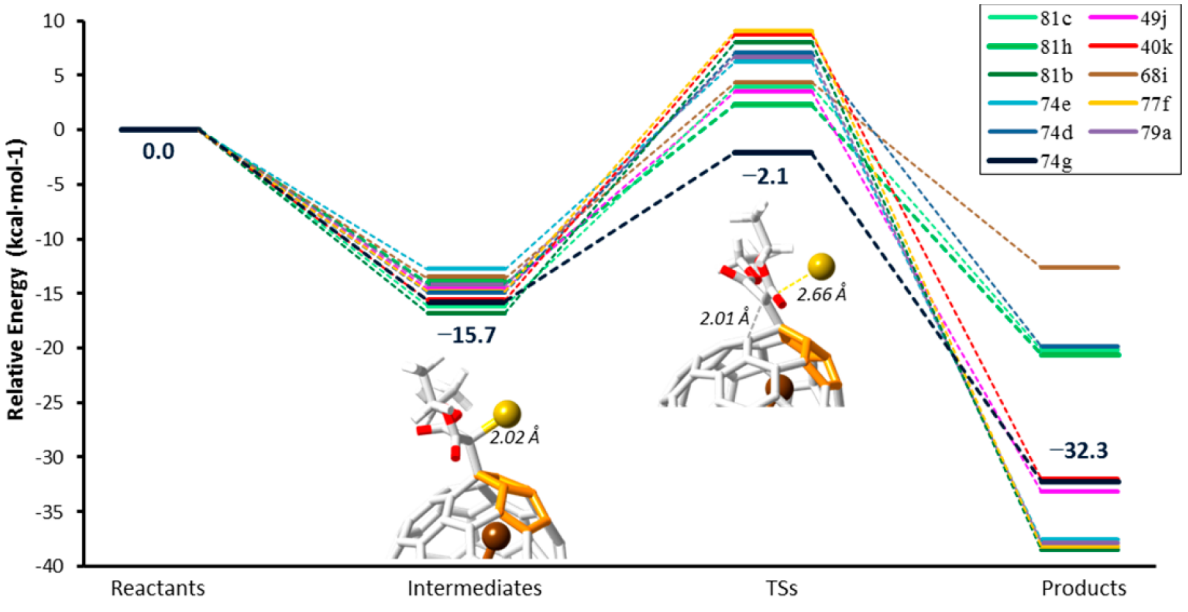

Figure 2. Plot of the relative energies of the different intermediates and transition states studied in this work for the Bingel–Hirsch addition on $Y_3N@C_s(39663)$-C_{82}, considering solvent effects (*o*-dichlorobenzene). Parts of the structures of the lowest-energy intermediate and TS are also depicted.

pentalene unit that can be activated through interaction with the internal metal atoms is larger. We found the products on bonds **l** and **m**, with relative energies of 0.0 and 0.7 kcal mol^{-1}, to be the lowest-energy monoadducts. These two so-similar values are in

dx.doi.org/10.1021/jo4014832 | J. Org. Chem. 2013, 78, 9986–9990

good agreement with the fact that the two bonds are related by symmetry in the empty C_s(51365)-C_{84} cage. At 2.3 and 5.0 kcal mol^{-1} higher energies, we found products **r** and **q**, respectively. It should be noted that also now the lowest-energy products correspond to adducts on the four [5,6] corannulene bonds around the pentalene motif. Monoadducts on the [6,6] bonds **y**, **v**, and **x**, which are far from the pentalene but activated by the metal atoms, show energies around 4.7−6 kcal mol^{-1} higher than adduct **l**. Other products show energies that are above 12 kcal mol^{-1} (Table 1).

Intermediates **79r**, **83s**, and **81t**, which are essentially isoenergetic within the error of the methodology, show the lowest energies. A large group of intermediates with energies between 1.4 and 2.5 kcal mol^{-1} are also observed: **81q**, **55u**, **83m**, **24y**, **77l**, **32w**, **24x**, **32v**, **83n**, and **81p**. Intermediates on the [6,6] pyrene-type and [5,5] pentalene-type bonds (**45x** and **78o**, respectively) appear at higher energies (Table 1). As for C_s(39663)-C_{82}, intermediates on 566 atoms are favored near the pentalene unit, while intermediates on 666 atoms are preferred far from the pentalene. Again, energy differences among the intermediates are not as significant as those among the products. As far as the TSs are concerned, **83s** is the one with the lowest energy (0.7 kcal mol^{-1} with respect to reactants) and the lowest barrier (17.3 kcal mol^{-1}). TS **81t** is found more than 2 kcal mol^{-1} above, and the other TSs show much larger energies and barriers (Table 1). Therefore, the monoadduct on bond **s** is proposed to be the single regioisomer observed experimentally if the Bingel−Hirsch reaction on $Y_3N@C_s$(51365)-C_{84} were to take place under kinetic control.

To sum up, the products of the Bingel−Hirsch reaction on the non-IPR fullerenes $Y_3N@C_{2n}$ ($2n$ = 82, 84) have been predicted. We have assumed that the reaction takes place under kinetic control, as recently observed for similar nitride EMFs. The two egg-shaped non-IPR cages in these EMFs are rather similar and intimately related. Besides, the nitride cluster has limited rotation around the N−M−pentalene axis. Therefore, similar behavior for the two EMFs is expected. All of the regioisomers analyzed show open-fulleroid structures where the functionalized C−C bond is broken. The energy differences among the intermediates are much smaller than those among the final products. The predicted products, which come from the lowest-energy intermediates and TSs, are monoadducts on [6,6] B-type bonds placed near the pentalene motif, as also found for the non-IPR EMF $Sc_3N@D_3$(6140)-C_{68}. Thus, we have shown that the Bingel−Hirsch addition presents analogous reaction paths on different non-IPR nitride EMFs.

COMPUTATIONAL METHODOLOGY

All of the stationary points were first calculated using the ADF 2009 code[19] with a Slater TZP-quality basis set and the BP86 functional.[20,21] In a second step, the most stable intermediates and TSs were reoptimized with the M06 functional[22] and the 6-31G** basis set (LANL2DZ for Y) using the Gaussian 09 code[23] and then evaluated with the PCM method[24] by single-point energy calculations at the M06/6-311G** (TZ for Y) level to take into account the solvent effects (see the Supporting Information for details).

ASSOCIATED CONTENT

Supporting Information

Additional results and figures related to the characterization of the potential energy surface. This material is available free of charge via the Internet at http://pubs.acs.org.

AUTHOR INFORMATION

Corresponding Authors

*E-mail: antonio.rodriguezf@urv.cat.
*E-mail: josepmaria.poblet@urv.cat.

Notes

The authors declare no competing financial interest.

ACKNOWLEDGMENTS

This work was supported by the Spanish Ministerio de Economía y Competitividad (Project CTQ2011-29054-C02-01) and the Generalitat de Catalunya (2009SGR462 and XRQTC). N.A. thanks the Spanish Ministerio de Economía y Competitividad for a doctoral fellowship.

REFERENCES

(1) Braun, K.; Dunsch, L.; Pipkorn, R.; Bock, M.; Baeuerle, T.; Yang, S. F.; Waldeck, W.; Wiessler, M. *Int. J. Med. Sci.* **2010**, *7*, 136.
(2) Lu, X.; Feng, L.; Akasaka, T.; Nagase, S. *Chem. Soc. Rev.* **2012**, *41*, 7723.
(3) Bottari, G.; de la Torre, G.; Guldi, D. M.; Torres, T. *Chem. Rev.* **2010**, *110*, 6768.
(4) Shu, C.; Corwin, F. D.; Zhang, J.; Chen, Z.; Reid, J. E.; Sun, M.; Xu, W.; Sim, J. H.; Wang, C.; Fatouros, P. P.; Esker, A. R.; Gibson, H. W.; Dorn, H. C. *Bioconjugate Chem.* **2009**, *20*, 1186.
(5) Rudolf, M.; Wolfrum, S.; Guldi, D.; Feng, L.; Tsuchiya, T.; Akasaka, T.; Echegoyen, L. *Chem.—Eur. J.* **2012**, *18*, 5136.
(6) Rodríguez-Fortea, A.; Balch, A.; Poblet, J. M. *Chem. Soc. Rev.* **2011**, *40*, 3551.
(7) Osuna, S.; Swart, M.; Solà, M. *Phys. Chem. Chem. Phys.* **2011**, *13*, 3585.
(8) Alegret, N.; Rodríguez-Fortea, A.; Poblet, J. M. *Chem.—Eur. J.* **2013**, *19*, 5061.
(9) Rodríguez-Fortea, A.; Alegret, N.; Balch, A. L.; Poblet, J. M. *Nat. Chem.* **2010**, *2*, 955.
(10) Hirsch, A.; Brettreich, M. *Fullerenes: Chemistry and Reactions*; Wiley-VCH: Weinheim, Germany, 2005.
(11) Feng, L.; Nakahodo, T.; Wakahara, T.; Tsuchiya, T.; Maeda, Y.; Akasaka, T.; Kato, T.; Horn, E.; Yoza, K.; Mizorogi, N.; Nagase, S. *J. Am. Chem. Soc.* **2005**, *127*, 17136.
(12) Chaur, M. N.; Melin, F.; Athans, A. J.; Elliott, B.; Walker, K.; Holloway, B. C.; Echegoyen, L. *Chem. Commun.* **2008**, 2665.
(13) Alegret, N.; Chaur, M. N.; Santos, E.; Rodríguez-Fortea, A.; Echegoyen, L.; Poblet, J. M. *J. Org. Chem.* **2010**, *75*, 8299.
(14) Slanina, Z.; Stobinski, L.; Tomasik, P.; Lin, H.-M.; Adamowicz, L. *J. Nanosci. Nanotechnol.* **2003**, *3*, 193.
(15) Zuo, T.; Walker, K.; Olmstead, M. M.; Melin, F.; Holloway, B. C.; Echegoyen, L.; Dorn, H. C.; Chaur, M. N.; Chancellor, C. J.; Beavers, C. M.; Balch, A. L.; Athans, A. J. *Chem. Commun.* **2008**, 1067.
(16) Mercado, B. Q.; Beavers, C. M.; Olmstead, M. M.; Chaur, M. N.; Walker, K.; Holloway, B. C.; Echegoyen, L.; Balch, A. L. *J. Am. Chem. Soc.* **2008**, *130*, 7854.
(17) Valencia, R.; Rodríguez-Fortea, A.; Clotet, A.; de Graaf, C.; Chaur, M.; Echegoyen, L.; Poblet, J. M. *Chem.—Eur. J.* **2009**, *15*, 10997.
(18) Rivera-Nazario, D. M.; Pinzón, J. R.; Stevenson, S.; Echegoyen, L. A. *J. Phys. Org. Chem.* **2013**, *26*, 194.
(19) te Velde, G.; Bickelhaupt, F. M.; Baerends, E. J.; Fonseca Guerra, C.; van Gisbergen, S. J. A.; Snijders, J. G.; Ziegler, T. *J. Comput. Chem.* **2001**, *22*, 931.
(20) Becke, A. D. *Phys. Rev. A* **1988**, *38*, 3098.
(21) Perdew, J. P. *Phys. Rev. B* **1986**, *33*, 8822.
(22) Zhao, Y.; Truhlar, D. *Theor. Chem. Acc.* **2008**, *120*, 215.
(23) Frisch, M. J.; Trucks, G. W.; Schlegel, H. B.; Scuseria, G. E.; Robb, M. A.; Cheeseman, J. R.; Scalmani, G.; Barone, V.; Mennucci, B.; Petersson, G. A.; Nakatsuji, H.; Caricato, M.; Li, X.; Hratchian, H. P.; Izmaylov, A. F.; Bloino, J.; Zheng, G.; Sonnenberg, J. L.; Hada, M.; Ehara, M.; Toyota, K.; Fukuda, R.; Hasegawa, J.; Ishida, M.; Nakajima, T.; Honda, Y.; Kitao, O.; Nakai, H.; Vreven, T.; Montgomery, J. A., Jr.;

Peralta, J. E.; Ogliaro, F.; Bearpark, M.; Heyd, J. J.; ; Brothers, E.; Kudin, K. N.; Staroverov, V. N.; Kobayashi, R.; Normand, J.; Raghavachari, K.; Rendell, A.; Burant, J. C.; Iyengar, S. S.; Tomasi, J.; Cossi, M.; Rega, N.; Millam, J. M.; Klene, M.; Knox, J. E.; Cross, J. B.; Bakken, V.; Adamo, C.; Jaramillo, J.; Gomperts, R.; Stratmann, R. E.; Yazyev, O.; Austin, A. J.; Cammi, R.; Pomelli, C.; Ochterski, J. W.; Martin, R. L.; Morokuma, K.; Zakrzewski, V. G.; Voth, G. A.; Salvador, P.; Dannenberg, J. J.; Dapprich, S.; Daniels, A. D.; Farkas, Ö.; Foresman, J. B.; Ortiz, J. V.; Cioslowski, J.; Fox, D. J. *Gaussian 09*; Gaussian, Inc: Wallingford, CT, 2009.

(24) Tomasi, J.; Mennucci, B.; Cammi, R. *Chem. Rev.* **2005**, *105*, 2999.